Journal of Catalysis **185,** 333–344 (1999)
Article ID jcat.1999.2519, available online at http://www.idealibrary.com on IDEAL®

Characterization of Spent MnO_2/CeO_2 Wet Oxidation Catalyst by TPO–MS, XPS, and S-SIMS

Safia Hamoudi, Faïçal Larachi,[1] Alain Adnot, and Abdelhamid Sayari

Department of Chemical Engineering and CERPIC, Université Laval, Ste-Foy, Québec G1K 7P4, Canada

Received October 15, 1998; revised January 27, 1999; accepted April 13, 1999

The surface modifications of MnO_2/CeO_2 catalyst during catalytic wet oxidation reaction were shown to be mainly due to carbonaceous deposits. Detailed characterization of the deposits was carried out using temperature-programmed oxidation coupled with mass spectrometry detection (TPO–MS), X-ray photoelectron spectroscopy, (XPS) and static secondary ion mass spectrometry (S-SIMS). The TPO–MS provided evidence that the nature of the carbonaceous deposits was dependent on the reaction temperature and time. The XPS investigation revealed the complex chemical composition of the organic material on the catalyst surface. The C1*s* region exhibited aromatic/graphitic, aliphatic, and oxygen-bearing carbon. The relative contribution of the aromatic/graphitic carbon increased with reaction time. The O1*s* region was composed of a strong signal attributable to the inorganic oxides and signals with moderate intensity stemming from adsorbed water, surface hydroxyl, and organic oxygen from alcohols or esters in agreement with the C1*s* peak reconstruction. The static SIMS analysis confirmed the existence of long aliphatic chains on the catalyst surface, together with aromatics of low polycondensation level indicating a low level of graphitization of the deposits.

Key Words: **oxidation; wastewater; oxide catalyst; carbonaceous deposit; deactivation; XPS; TPO; SIMS.**

INTRODUCTION

Catalytic wet oxidation (CWO) is a subcritical abatement method that uses dissolved molecular oxygen to catalytically destroy target organic pollutants contained in wastewater streams. Ideally, provided that temperature and pressure are sufficiently high, any organic species undergoes complete mineralization. The use of solid catalysts not only allows oxidative treatments to be accomplished under moderate severity (90–150°C; 0.1–2 MPa O_2) (1) but also offers a versatile process wherein the catalyst, unlike a homogeneous one, may be easily recovered and eventually reused. CWO involving solid catalysts has therefore attracted attention as an alternate method for cleaning wastewaters, and various solid catalysts have been tested on model pollutant solutions (2–5).

Previous work on heterogeneously catalyzed oxidation of phenolic solutions revealed the formation of carbonaceous polymeric deposits on the catalysts surface during the reaction (4, 6, 7). This resulted in catalyst deactivation via physical blockage of active sites by these high-molecular-weight carbonaceous materials. However, despite the fact that the simultaneous formation of heavy polymeric products in wet oxidation is clearly evidenced, their chemical nature, their mechanism of formation, and their deactivating mode are still unclear or unknown. Hence, the understanding of the chemical composition of these surface species is a prerequisite for avoiding, or at least delaying, their formation.

Among the numerous methods employed to characterize carbonaceous deposits that are frequently encountered in the petroleum refining processes, temperature-programmed oxidation (TPO) is among the most commonly used techniques (8–10). In this bulk technique, an oxygen-containing inert gas flows over a deactivated (coked) catalyst at a program-controlled increasing temperature. By monitoring the gas-phase composition versus time, information on the nature and the reactivity of the carbonaceous deposits can be obtained. Indeed, in TPO, oxygen is consumed via different reactions: carbon atoms are converted to carbon dioxide, hydrogen atoms to water, and eventually metals to oxides. The position of the oxidation peaks provides information on the temperature required for the deposits to burn off and thus on how easily the catalyst can be regenerated.

X-ray photoelectron spectroscopy (XPS) has been successfully employed to provide useful surface analysis of nearly every type of material (11). Thus, it seemed worthwhile to use this technique to probe the nature of the carbonaceous deposits formed during CWO. Static secondary ion mass spectrometry (S-SIMS) can also provide valuable information on the nature of chemisorbed species (12–14) and deactivating carbonaceous layers on catalyst surfaces (15). The advantages of this technique lie in its high sensitivity and detailed molecular structural information. SIMS and XPS, therefore, make it possible to study the outermost layers of the catalyst surface with a low detection limit, giving

[1] To whom correspondence should be addressed. E-mail: flarachi@gch.ulaval.ca.

0021-9517/99 $30.00

valuable insights into surface molecular structure (16, 17). These techniques were thus used in the current work to fingerprint the evolution of the carbonaceous deposits at different stages of the CWO reaction conducted at different temperatures over MnO_2/CeO_2 catalyst.

EXPERIMENTAL

Materials and Procedures

Phenol (99+% purity) was purchased from BDH Co. and was used without further purification. Manganese and cerium composite oxide with a molar ratio of 7/3 was prepared by coprecipitation from an aqueous solution of manganese (II) chloride (Fisher Scientific Co.) and cerium (III) chloride (Sigma Chemical Co.) followed by calcination under flowing air at 350°C for 3 h (18). The obtained powder was crushed and sieved to produce particle sizes with a weight-mean value equal to 63 μm. The BET surface area of the catalyst (107 m^2/g) was determined using N_2 adsorption and the BET model. The adsorption isotherm was measured using an automated volumetric adsorption analyzer, Omnisorp 100, from Coulter. The carbon content on the catalyst surface was quantified by CHN elemental analysis (Carlo Erba, Model 1106). The oxidation tests were carried out in a stainless steel autoclave operated batchwise at temperatures ranging within 80–130°C under an oxygen partial pressure of 0.5 MPa. The initial phenol concentration was 1–10 g/L and the catalyst loading 1–5 g/L. The extent of the conversion was monitored by measuring the total organic carbon (TOC) content of filtered aliquots of reaction samples withdrawn at different reaction times. A TOC Analyzer 5050 from Shimadzu was used. The experimental procedure was already described elsewhere in detail (6) and will not be reported here for conciseness.

TPO–MS Measurements

The organic species adsorbed on the catalyst during CWO reaction were characterized by TPO using an Altamira AMI1 instrument. In a typical TPO experiment, about 60 to 100 mg of spent catalyst was loaded in a U-shaped quartz microreactor that was then installed in a furnace coupled to a temperature controller–programmer. The catalyst was first exposed to flowing helium (30 mL/min) and the temperature was raised at a rate of 10°C/min up to 120°C and was kept at this temperature for 20 min before cooling down to room temperature. This first pretreatment step was conducted at a relatively low temperature in order to remove physisorbed water from the catalyst sample, but without thermally modifying the nature of the deposit. Subsequently, the catalyst was heated under a flowing gas mixture of 5% oxygen in helium at a rate of 8°C/min up to 500°C. Analysis of the gaseous burn off products was performed by thermal conductivity (TCD) and by mass spectrometry using a transpector quadrupole from Leybold Inficon, Inc. The Altamira instrument and the mass spectrometer were both interfaced to personal computers for data acquisition.

XPS and Static SIMS Measurements

XPS spectra for fresh and used catalysts were recorded using a Vacuum Generator Scientific ESCALAB Mark II system. A Mg K_α anode ($h\nu = 1253.6$ eV) was used as the X-ray source. Kinetic energies of photoelectrons were measured using a hemispherical electrostatic analyzer working in the constant pass energy mode. Survey (0–1000 eV) and detailed spectra (C1*s*; Mn2*p*; Ce3*d*; O1*s*) were acquired at pass energy of 50 eV and 10–20 eV, respectively. Correspondingly, the resolutions were 1 eV and 0.05–0.1 eV. In order to correct for the sample charging, the binding energies (B.E.) of core levels in the observed XPS spectra were referenced to Au4$f_{7/2}$ core level for gold-sputtered fresh catalyst sample (B.E. = 84 eV) and Mn2$p_{3/2}$ core level in MnO_2 (B.E. = 641.9 eV) for the used samples. The experiments were run at room temperature in the analyzing chamber under a pressure of less than 10^{-6} mbar. Data processing was performed using a modified version of software developed by Hughes and Sexton (19).

The static SIMS spectra of MnO_2/CeO_2 wafers were recorded on a Vacuum Generator SIMSLAB instrument equipped with a MM12-12 mass spectrometer, using Ar^+ ions with a current density <1 nA/cm^2 and an energy of 1 keV. The total ion dose after analysis was less than 5.10^{12} ions/cm^2.

Curve Fitting of XPS Spectra

The overall C1*s* and O1*s* XP spectra were curve fitted into sets of individual line components stemming from species with different chemical and bonding environments. The optimum number of such lines was obtained using statistical procedures that establish the minimum number of peaks leading to statistically meaningful fits (20, 21). A series of weighted least-squares fits was adjusted by incrementally adding peaks one at a time to the XP C1*s* and O1*s* spectra for a given spent MnO_2/CeO_2 sample. Starting with a single peak, the number of peaks was increased stepwise, and the corresponding adjustable parameters were χ^2 fitted. The goodness-of-fit of the spectral data to the model was estimated by evaluating the reduced χ^2 (sum of squared residuals normalized by the number of degrees of freedom, ν), the χ^2 probability function $Q(\chi^2 \mid \nu)$, and the normal quantile–quantile plot of residuals. $Q(\tau \mid \nu)$ is the probability that the observed χ^2 will exceed τ by chance. The 95% confidence limits of the χ^2 distribution correspond to Q values of 0.005 and 0.995; for a perfect fit $Q = 0.5$ and $\chi^2 \to 1$. Any model giving Q values outside the range 0.005–0.995 should be rejected.

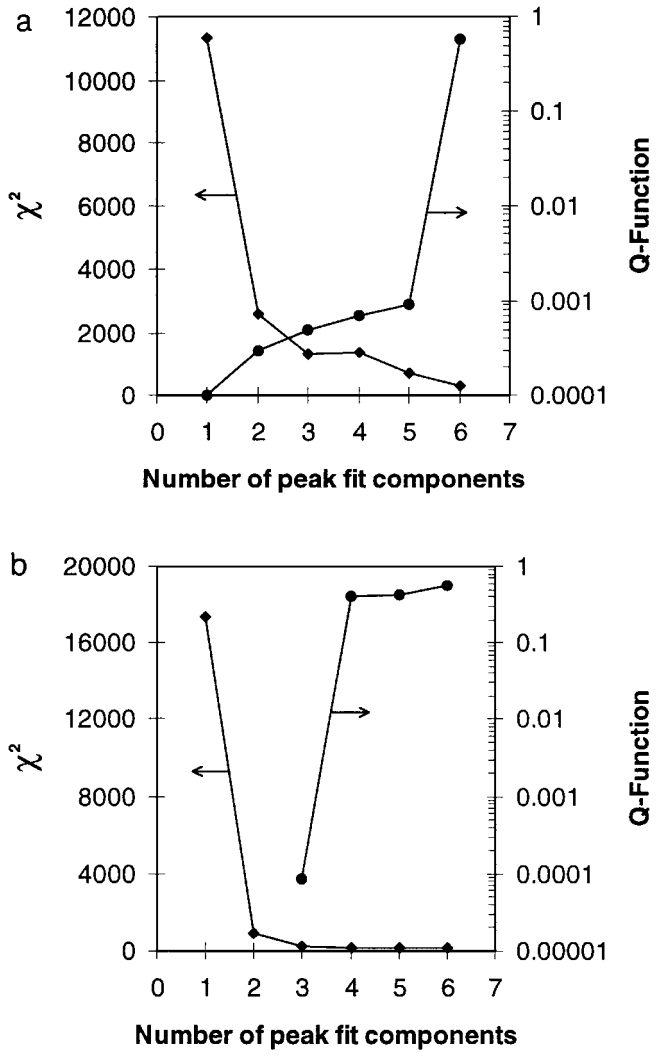

FIG. 1. Reduced χ^2 and $Q(\chi^2 \mid \nu)$ versus number of peak components used in curve fitting (a) C1*s* and (b) O1*s* XP spectra.

Figures 1a and 1b are typical plots of χ^2 and Q versus the incremental number of peaks included in the curve fitting of the C1*s* and O1*s* spectra, respectively. For both cases, χ^2 dropped sharply as the number of peaks increased from one to six. With five peaks or less, the Q value for C1*s* was below 0.001. As the six peak was added, the Q value jumped to 0.57, indicating the occurrence of an almost perfect match between the experimental spectrum and the sum of the six peak components. Fitting the O1*s* signal exhibited similar, but less dramatic behavior. Based on literature data, and on prior knowledge of the chemical functionalities generated during the oxidation of phenol aqueous solutions, reasonable assignments were given to all six oxygen and carbon species corresponding to individual components.

Curve fitting of the C1*s* region was performed, after a linear background was subtracted over a constant range of 20 eV, using reported binding energies for the C1*s* core level for aromatic/graphitic, aliphatic, or carbon adjacent to carbon atoms bonded to oxygen (β-carbon) and oxygen-bearing carbon species (6, 22, 23). A mixture of Lorentzian and Gaussian curves was used. The full-width at half-maximum (FWHM) of the peaks corresponding to aromatic, aliphatic, and oxygen-bearing carbon was constrained to the same value, but the starting value of 1.85 eV was allowed to change until the best fit was obtained. For the Π–Π^* shake-up contribution, a FWHM = 3 eV was used (22–24).

For the O1*s* spectra, the curve fitting was performed after a linear background was subtracted over a constant range of 16 eV. The FWHM was the same for all six components. It was initialized at 1.7 eV (23) and was allowed to vary within ±20%. Oxygen species with O1*s* B.E. of 529.2 ± 0.2 and 530.0 ± 0.2 eV were assigned to CeO_2 and MnO_2, respectively (25, 26). These B.E. values were determined based on the decomposition of the O1*s* spectrum for fresh MnO_2/CeO_2. In comparison to pure ceria (B.E. = 528.6), the O1*s* peak attributed to cerium in mixed manganese/cerium oxides shifted upward by ca. 0.6 eV. Higher Ce O1*s* B.E. values were also observed for silica-supported ceria where shifts of up to 1.7 eV were observed for samples containing less than 11 wt% ceria (26). All O1*s* spectra for used catalysts were fitted using as constraint that the ratio of oxygen species originating from MnO_2 and CeO_2 be equal to the corresponding surface Mn to Ce ratios. The other four oxygen components involved in the curve fitting procedures were attributed to surface hydroxyls (531.4 ± 0.2 eV) and adsorbed molecular water (532.4 ± 0.2 eV) (23, 27) and to two organic species. The latter were composed of oxygen single bonded to carbon alcohol, ether, or an ester function (532 ± 0.2 eV) and oxygen double bonded to carbon from a carbonyl group (533.5 ± 0.2 eV) (23, 27).

RESULTS AND DISCUSSION

CWO Tests

Typical phenol degradation profiles over MnO_2/CeO_2 in the range 80–130°C under constant oxygen partial pressure (0.5 MPa), 1 g/L initial phenol concentration, 5 g/L catalyst loading, are depicted in Fig. 2a as TOC conversion versus time. While complete removal of the pollutant was achieved within 30 min at 130°C (TOC reduction = 98%), at 80°C more than 120 min was required to reach comparable results (TOC reduction = 97%). For more concentrated phenol solutions (5–10 g/L) and/or a lower catalyst loading (1–2.5 g/L), it was not possible to achieve complete TOC conversion even after prolonged contact times (Fig. 2b). The degradation profiles leveled off and the reaction stopped despite the availability of liquid reactant and oxygen. In our earlier work (6, 7), it was clearly demonstrated through kinetic tests and thorough characterization of the catalyst

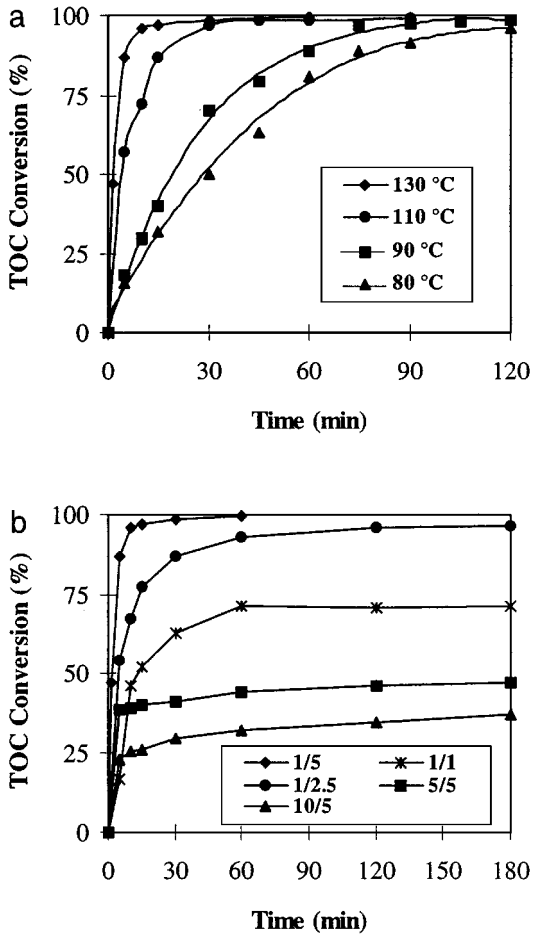

FIG. 2. (a) Effect of temperature on phenol CWO over MnO_2/CeO_2 in terms of TOC conversion. (b) Effect of phenol initial concentration and catalyst loading on phenol CWO in terms of TOC conversion at 130°C (x/y in the legend refers to $[phenol]_0/[catalyst]$ ratio).

(CHN elemental analysis, TPO, and XPS) that this reaction break down was due to the accumulation of carbonaceous deposits that irreversibly adsorbed on the catalyst surface, thus blocking its active sites.

TPO Analysis

Representative TPO–MS data illustrating the time evolution of carbon dioxide and water, as well as oxygen consumption during temperature-programmed burning off of a partially deactivated catalyst sample, are shown in Fig. 3. Oxygen consumption was almost mirrored by the formation of CO_2. The carbonaceous deposit was completely removed below 300°C. The CO_2 production profile comprised three distinct features: a sharp peak between 200 and 210°C and two broad peaks with maxima around 250 and 280°C, respectively. This indicates that the carbonaceous deposit is of complex structure with components burning at different temperatures. The H_2O production profile exhibited a bell shape starting always after the appearance of the sharp CO_2 peak. This may indicate that the carbonaceous species with the highest reactivity with oxygen are poorly hydrogenated.

TPO–MS experiments on used catalyst samples were performed to monitor the evolution of the deposits at different stages of the reaction. Figures 4A, 4B and Figs. 4C, 4D depict the CO_2 and H_2O production profiles corresponding to catalyst samples withdrawn at different reaction times during CWO at 90 and 110°C, respectively. From the CO_2 production profiles, it is seen that the features of the combustion peaks, in terms of peak area and shape, indicate that the amount as well as the nature of the carbonaceous deposit evolved during the CWO reaction. The evolution was faster at the higher CWO temperature where the final shape of the combustion peak was obtained just after 30 min of reaction, while at 90°C this shape was obtained after 60 min of reaction. The shape of water production profiles did not change with time, indicating that, irrespective of the time at which the catalyst was sampled, the only hydrogenated species corresponded to those burning at high temperature (>250°C).

The amount of water produced increased with CWO reaction time as the deposits accumulated further. The oxygen consumption corresponding to the TPO runs of Figures 4A–4D is plotted against TOC conversion in Fig. 5a. As seen, this oxygen consumption increases monotonically with TOC conversion. Furthermore, at constant TOC conversion, oxygen consumption was higher for the lower CWO temperature. A similar conclusion is reached when the catalyst carbon content is plotted against TOC conversion (see Fig. 5b), indicating that the oxygen consumption is closely cross-correlated to the amount of carbonaceous deposits building up on the catalyst surface (28). Moreover, a lesser amount of carbonaceous deposit is formed at higher

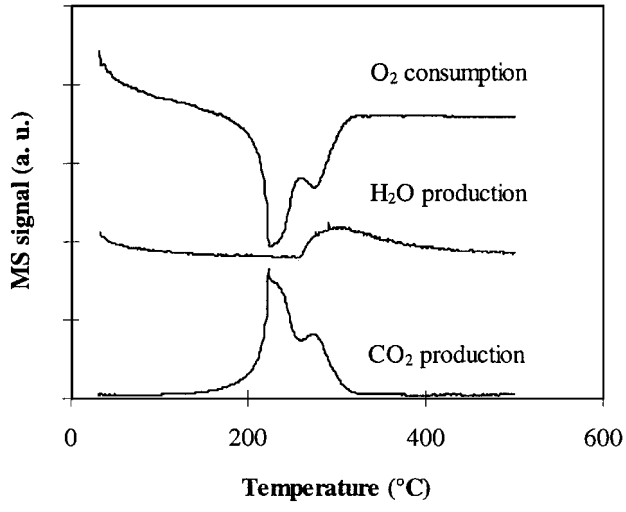

FIG. 3. TPO–MS (O_2, CO_2, and H_2O) profiles for used MnO_2/CeO_2 catalyst.

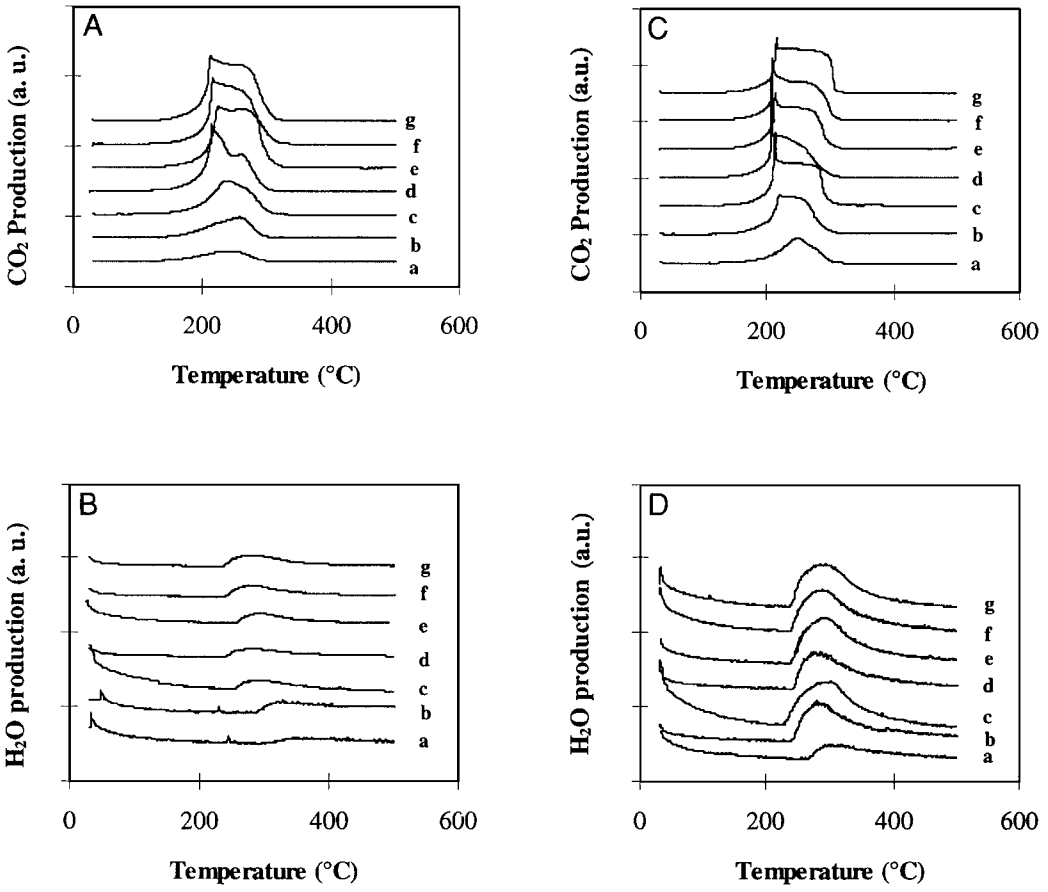

FIG. 4. TPO of catalyst samples withdrawn at different CWO reaction times at 90 and 110°C. (A, B) CO_2 and H_2O production during TPO (90°C): a, 5 min; b, 10 min; c, 15 min; d, 30 min; e, 45 min; f, 60 min; and g, 120 min. (C, D) CO_2 and H_2O production during TPO (110°C): a, 5 min; b, 10 min; c, 15 min; d, 30 min; e, 45 min; f, 60 min; and g, 90 min.

temperature, which indicates that CWO yielded a better phenol mineralization.

XPS Analysis

Oxidation State of Surface Mn and Ce

Examination of the Mn2*p* and Ce3*d* spectra of a fresh gold-sputtered manganese/cerium oxide catalyst allowed the determination of the oxidation state of surface manganese and cerium oxides. With reference to the Au4$f_{7/2}$ XPS line at 84 eV, binding energies of 641.9 and 882.6 eV were found for Mn2$p_{3/2}$ and Ce3$d_{5/2}$ XPS lines, respectively (Figs. 6A and 6B). These values are in good agreement with those reported in the literature (29–36) for MnO_2 and CeO_2, i.e., 642 ± 0.2 and 882.2 ± 0.4 eV for Mn2$p_{3/2}$ and Ce3$d_{5/2}$ core levels, respectively. Furthermore, according to Burroughs *et al.* (37) and Creaser *et al.* (38), the envelope of the Ce3*d* spectrum, shown in Fig. 6B, is characteristic of cerium (IV) oxide. To study the oxidation state changes of the catalytic active phase (Mn and Ce oxides) that may occur during the course of the CWO reaction, measurements of the binding energies of Mn2$p_{3/2}$ and Ce3$d_{5/2}$ electrons were undertaken for eight samples used in CWO for different periods of time in the temperature range of 80 to 130°C. The corresponding spectra are presented in Figs. 6A and 6B (for Mn2$p_{3/2}$ and Ce3$d_{5/2}$, respectively). With reference to the most intense C1*s* peak positioned at 285 eV, the observed lines remained unshifted, suggesting that the oxidation state of the transition metals did not change during the reaction. Furthermore, regardless of energy referencing, the difference between Mn2$p_{3/2}$ and Ce3$d_{5/2}$ lines, evaluated to be 240.7 ± 0.1 eV for the fresh catalyst sample, remained unchanged for the eight tested samples. The constancy of this difference in binding energies between Mn2$p_{3/2}$ and Ce3$d_{5/2}$ rules out unambiguously any change in the oxidation state of the oxides as well as any electron transfer from one oxide to the other during the course of the CWO reaction.

The effects of CWO temperature and reaction time on the relative amounts of surface Mn and Ce are clearly shown in Figs. 6A and 6B where decreases in peak area and intensity for both metals are observed. At a given temperature, the relative amounts of both metals decreased with increasing CWO reaction time. This decrease was more

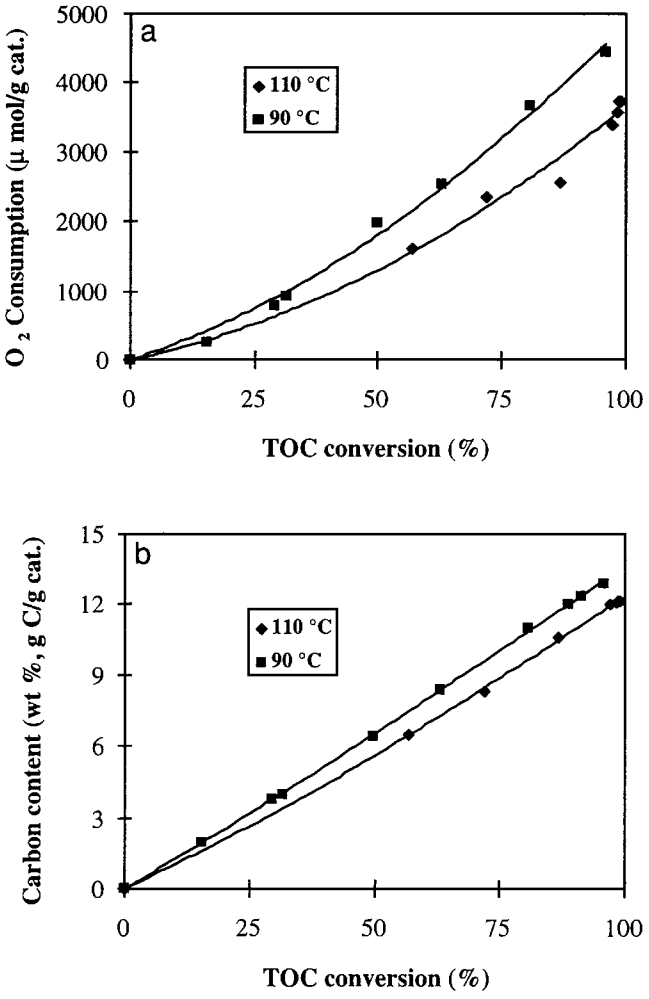

FIG. 5. (a) O_2 consumption versus TOC conversion for samples withdrawn at 90 and 110°C. (b) Catalyst carbon content versus TOC conversion for samples withdrawn at 90 and 110°C (lines show trends).

pronounced for Ce, particularly at higher CWO temperatures, presumably because the carbonaceous material preferentially builds up on the cerium oxide sites.

Chemical Nature of the Carbonaceous Deposits

Figure 7 presents the O1*s* and C1*s* XPS spectra recorded under the same conditions as those in Fig. 4. Figure 7A shows an interesting evolution of the O1*s* peak shape. In fact, as the CWO reaction time increases, the shoulder at high binding energy attributed mainly to organic oxygen, barely detectable for the fresh catalyst, becomes more and more prominent, indicating an important accumulation of organic material on the catalyst surface. Consistent with these findings, the plots in Fig. 7B indicate an increase in the relative surface carbon content during the CWO reaction. Table 1 presents the surface carbon content for fresh and used catalyst samples withdrawn after 30 and 90 min of CWO reaction at 80–130°C. In agreement with

TABLE 1

Surface Carbon Content (%) of Fresh and Used Catalysts as Determined by XPS

CWO temp (°C) (time in min)	Carbon (% atomic)	TOC conversion (%)
Fresh	2.5	—
80 (90)	56.6	91.7
90 (90)	62.2	97.3
110 (90)	56.8	98.9
130 (30)	45.0	98.6

Fig. 7B, the carbon content increased from ca. 2.5 atom% for the fresh catalyst to ca. 45–60 atom% of the uppermost layers of the catalyst during reaction. Furthermore, detailed examination of the C1*s* region of the XPS spectra gave

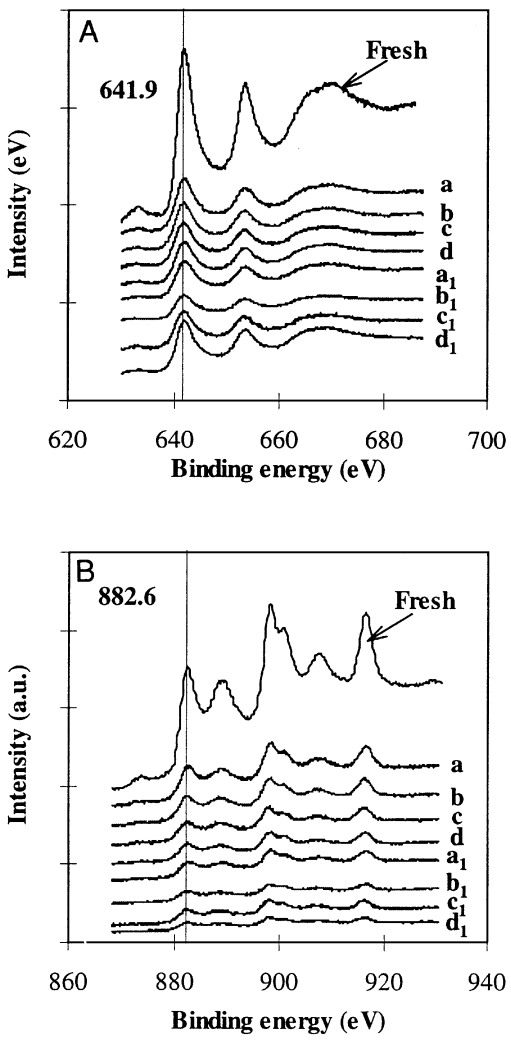

FIG. 6. Mn 2*p* (A) and Ce 3*d* (B) XPS spectra for fresh and used catalyst samples; (80°C) a, 5 min; a_1, 75 min; (90°C) b, 5 min; b_1, 90 min; (110°C) c, 5 min; c_1, 90 min; (130°C) d, 1.5 min; d_1, 30 min.

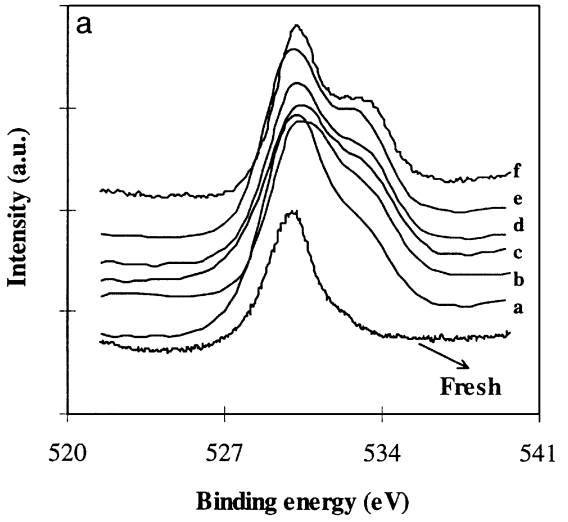

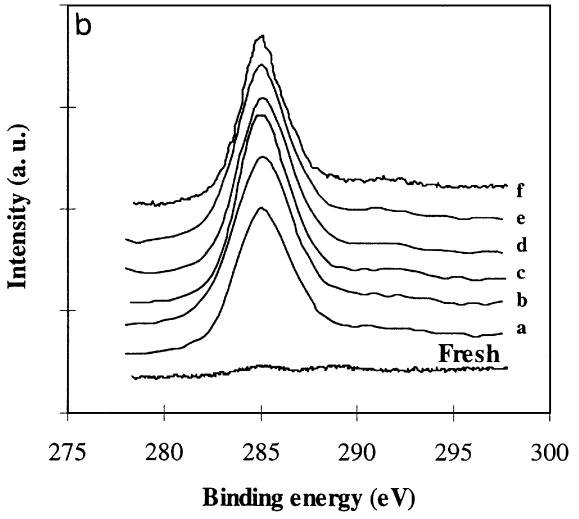

FIG. 7. O1*s* (A) and C1*s* (B) XPS spectra (reaction at 110°C); a, 5 min; b, 10 min; c, 15 min; d, 30 min; e, 45 min; f, 90 min.

corroborating evidence of a multicomponent peak corresponding to different chemical functionalities. The specific contribution of each carbon species can be separated by means of peak reconstruction and curve fitting as discussed earlier.

C1s core level. A typical C1*s* reconstructed spectrum is presented in Fig. 8a. It indicates that, among the six contributing peaks, only four had relatively high intensity, the two other being quite weak. As illustrated in Fig. 8b, the validity of the proposed six-peak fit was justified by an analysis of the residuals (39) using a normal standard quantile–quantile plot of the residuals for C1*s*. As seen, the residual plot exhibited high fidelity to a straight line, indicating that the residuals are normally distributed.

Tables 2 and 3 summarize the results obtained at four CWO temperatures for short and long reaction times, respectively. The aromatic/graphitic carbon (B.E. = 284.4 eV) accounted for ca. 18–33% of the total peak area, while the highest contributions (40–51%) were attributable to the aliphatic β-carbon with oxygen as next neighbor. The oxygen-bearing carbon, mainly from alcohol or ether origin, represented 16–25% of the C1*s* peak area. Small but significant contributions (6–8% of the overall C1*s* peak) of the Π–Π^* shake-up signal were also observed. This signal was detected only on surfaces with predominantly graphitic/aromatic carbon species. The shake-up satellite is caused by Π–Π^* transitions in the aromatic region, activated by the C1*s* photoelectron (40). The intensity of this satellite can be a good indicator of the amount of aromatics on the surface as reported by Kelemen *et al.* (41). These authors showed that the relative intensity of the Π–Π^* peaks correlates with the relative amount of aromatic

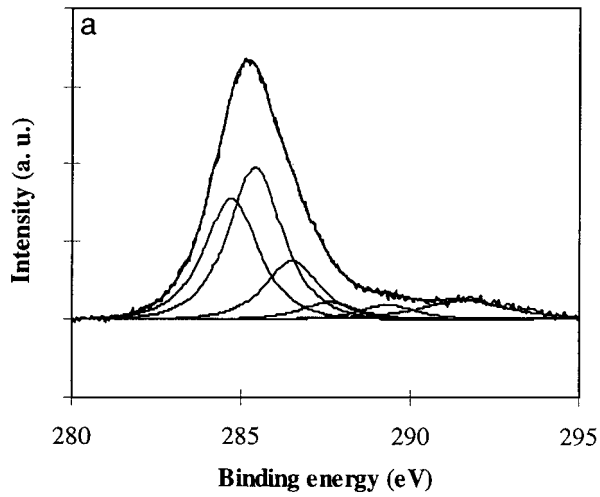

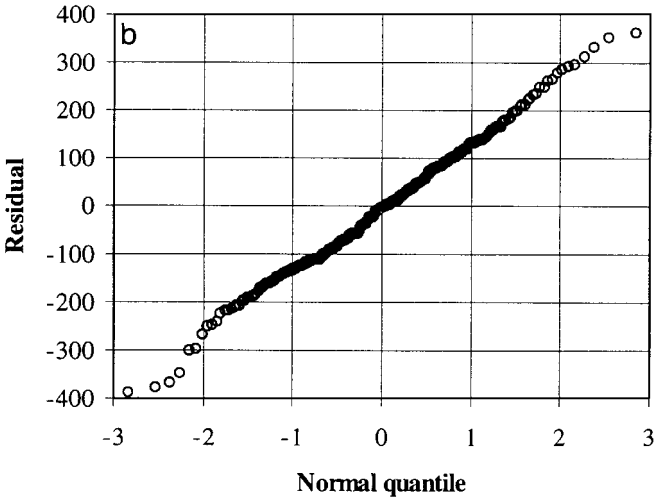

FIG. 8. (a) C1*s* XPS peak reconstruction for catalyst sample withdrawn after 30 min of CWO reaction at 130°C. (b) Normal quantile–quantile plot for the residuals in the C1*s* curve fitting.

TABLE 2

C1*s* XPS Data after Short Reaction Times: B.E.s and Relative Intensities of C1*s* Species

CWO Temp. (°C)	Time (min)	C content (% atomic)	Peak position (eV)	Assignment	Contribution to total C content (%)
80	5	28	284.4	Graph/aromatic	23.7
			285.1	Aliphatic/β-C	42.9
			286.2	C–OH; C–O–C	13.0
			287.4	C=O	2.4
			289.0	COOH; COOR	9.8
			291.4	Π–Π* shake up	7.9
90	5	42.7	284.4	Graph/aromatic	19.3
			285.1	Aliphatic/β–C	50.7
			286.3	C–OH; C–O–C	15.2
			287.4	C=O	3.6
			289.1	COOH; COOR	4.4
			291.4	Π–Π* shake up	6.6
110	5	48.6	284.3	Graph/aromatic	23.8
			285.1	Aliphatic/β–C	45.5
			286.3	C–OH; C–O–C	15.4
			287.4	C=O	3.2
			288.9	COOH; COOR	3.3
			291.4	Π–Π* shake up	8.6
130	1.5	46.8	284.4	Graph/aromatic	18.2
			285.1	Aliphatic/β–C	49.6
			286.3	C–OH; C–O–C	14.9
			287.4	C=O	3.8
			289.1	COOH; COOR	4.9
			291.4	Π–Π* shake up	8.6

carbon. Using their correlation, the mean relative content in aromatic carbon for all samples analyzed in the current work was found to be ca. 38%. It is noteworthy to point out that in all cases the contribution of aliphatic oxygenated carbon was always the highest, and the relative amount of the aromatic/graphitic carbon increased with CWO reaction time, while the other contributions remained almost constant.

O1s core level. As presented in Fig. 9a, the O1*s* spectra were fitted to 6 specific peaks. Similar to C1*s* spectra, the same goodness-of-fit criteria were used for the O1*s* spectra. The plot of residuals confirm a randomly distributed error with zero mean (Fig. 9b). As presented in Tables 4 and 5, the O1*s* peak fitting revealed a strong signal from the manganese oxide accounting for 43 to 62% of the total area of the whole peak. Oxygen from cerium oxide accounted for only 8–32% of the O1*s* peak area. Furthermore, both inorganic oxygen contributions decreased with increasing reaction time for all the CWO temperatures investigated, except for 130°C where they preserved the same values. Surface OH and water totaling ca. 4–10% of the overall peak area for short reaction times decreased slightly at long reaction times. On the contrary, the amount of adsorbed water increased with reaction time. The contribution of the oxygen single-bonded to carbon increased with CWO reaction time more significantly at 80 and 90°C than at higher temperatures. Oxygen double-bonded to carbon exhibited a modest contribution at low CWO temperature with a tendency to increase with reaction time.

SIMS Analysis

Static SIMS is a suitable method that supplies detailed information on the surface chemistry of finely divided and porous carbonaceous material and on adsorbed organic molecules (40, 42). It was also applied to identify relevant surface species occurring during catalytic reactions (43, 44). Usually, various types of ions detected by SIMS can be directly related to the substrate or to some of its fragments. In the present study, as the exact chemical nature of the substrate investigated (carbonaceous deposits) was unknown, the different cluster ions detected were assigned to groups of similar structures such as aliphatics, aromatics, and oxygenated carbon as revealed by the XPS analysis. SIMS spectra are inherently difficult to quantify particularly for real samples such as our current materials. Up to now, most attempts on SIMS quantification were carried out using well-characterized materials. Nevertheless, the proportions

TABLE 3

C1*s* XPS Data after Long Reaction Times: B.E.s and Relative Intensities of C1*s* Species

CWO Temp. (°C)	Time (min)	C content (% atomic)	Peak position (eV)	Assignment	Contribution to total C content (%)
80	75	55.8	284.4	Graph/aromatic	33.2
			285.1	Aliphatic/β-C	39.6
			286.3	C–OH; C–O–C	14.2
			287.8	C=O	1.8
			289.1	COOH; COOR	3.1
			291.4	Π–Π* shake up	8.0
90	90	62.8	284.4	Graph/aromatic	30.9
			285.1	Aliphatic/β–C	38.8
			286.3	C–OH; C–O–C	14.8
			287.4	C=O	4.3
			289.1	COOH; COOR	3.7
			291.4	Π–Π* shake up	7.6
110	90	56.8	284.3	Graph/aromatic	29.5
			285.1	Aliphatic/β–C	43.7
			286.3	C–OH; C–O–C	13.3
			287.4	C=O	2.3
			288.9	COOH; COOR	3.5
			291.4	Π–Π* shake up	7.7
130	30	45.0	284.4	Graph/aromatic	22.0
			285.1	Aliphatic/β–C	46.5
			286.3	C–OH; C–O–C	14.8
			287.4	C=O	4.9
			289.1	COOH; COOR	4.3
			291.4	Π–Π* shake up	7.4

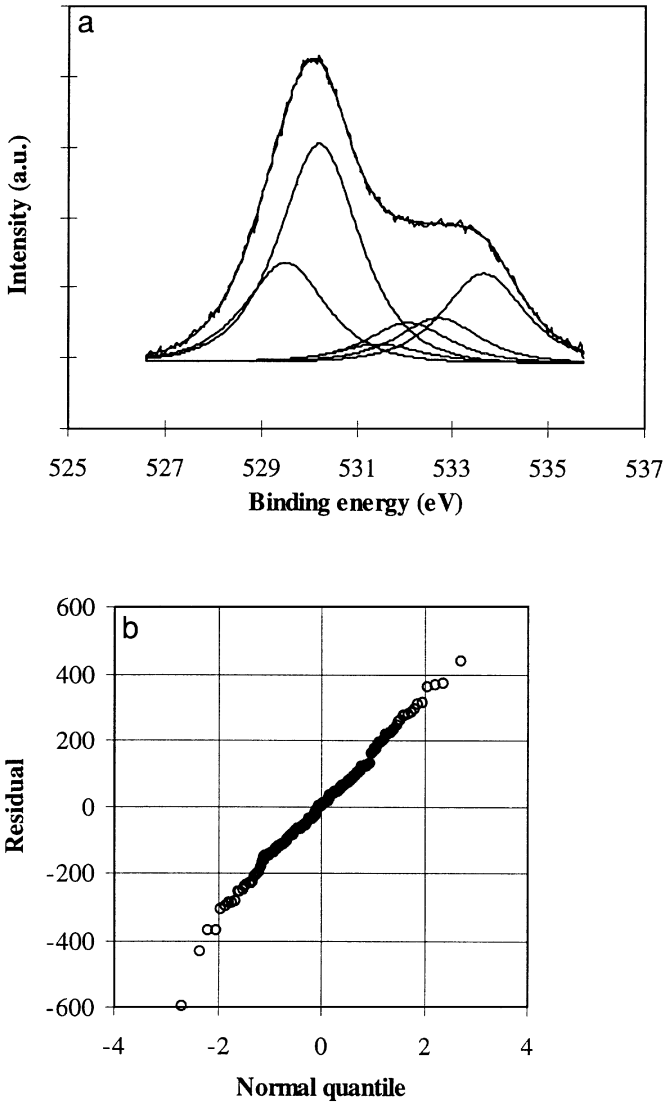

FIG. 9. (a) O1*s* XPS peak reconstruction for catalyst sample withdrawn after 30 min of CWO reaction at 130°C. (b) Normal quantile–quantile plot for the residuals in the O1*s* curve fitting.

of each SIMS-identified chemical group can give an overall topography of these carbonaceous deposits.

Positive Ion Spectra

The positive ion spectra (m/z 0–40) of MnO_2/CeO_2 catalysts used in CWO reactions at different temperatures and after achieving complete TOC conversion are given in Fig. 10. The peak at m/z 23 was due to sodium remaining from the precipitation step of the catalyst preparation. Clusters of ions between m/z 12 and m/z 15 assigned to CH_x^+ ($x = 0$–3) indicated the presence of aliphatic surface compounds. Those with m/z between 24 and 40 were attributed to species such as C_2^+ m/z 24; $C_2H_x^+$ ($x = 1-3$) = m/z 25–27; $C_2H_4^+/CO^+ = m/z$ 28; $C_2H_5^+/CHO^+ = m/z$ 29;

TABLE 4

O1*s* XPS Data after Short Reaction Times: B.E.s and Relative Intensities of O1*s* Species

CWO Temp. (°C)	Time (min)	O content (% atomic)	Peak position (eV)	Assignment	Contribution to total O content (%)
80	5	49.9	529.2	CeO_2	31.7
			530.2	MnO_2	54.7
			531.7	OH	3.8
			532.3	C=O (COOR)	3.5
			532.5	H_2O	2.6
			533.7	C–O (C–OH; COOR)	3.6
90	5	43.1	529.2	CeO_2	24.9
			529.9	MnO_2	50.4
			531.6	OH	4.8
			532.0	C=O (COOR)	6.5
			532.8	H_2O	3.6
			533.5	C–O (C–OH; COOR)	7.8
110	5	36.8	529.0	CeO_2	18.6
			529.8	MnO_2	48.5
			531.5	OH	10.0
			532.1	C=O (COOR)	1.9
			532.6	H_2O	8.0
			533.4	C–O (C–OH; COOR)	12.7
130	1.5	38.8	529.2	CeO_2	17.5
			529.9	MnO_2	52.8
			531.6	OH	7.5
			531.8	C=O (COOR)	3.5
			532.6	H_2O	6.3
			533.6	C–O (C–OH; COOR)	12.5

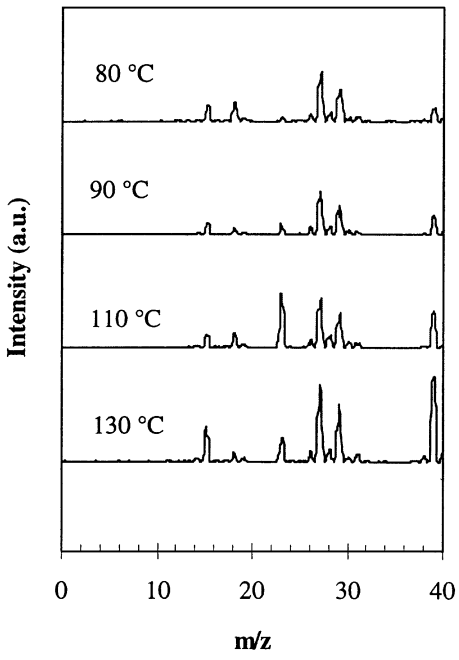

FIG. 10. S-SIMS spectra for catalyst samples withdrawn at different CWO temperatures: Positive secondary ions.

TABLE 5

O1*s* XPS Data after Long Reaction Times: B.E.s and Relative Intensities of O1*s* Species

CWO Temp. (°C)	Time (min)	O content (% atomic)	Peak position (eV)	Assignment	Contribution to total O content (%)
80	75	32.9	529.4	CeO_2	19.5
			530.2	MnO_2	43.3
			531.5	OH	3.4
			532.1	C=O (COOR)	7.8
			532.7	H_2O	8.6
			533.6	C–O (C–OH; COOR)	17.5
90	90	29.3	529.2	CeO_2	17.2
			529.9	MnO_2	33.8
			531.2	OH	7.9
			531.8	C=O (COOR)	8.0
			532.6	H_2O	14.8
			533.4	C–O (C–OH; COOR)	18.2
110	90	32.9	529.0	CeO_2	12.9
			529.9	MnO_2	43.2
			531.0	OH	5.7
			531.8	C=O (COOR)	9.3
			532.3	H_2O	10.1
			533.5	C–O (C–OH; COOR)	18.8
130	30	41.4	529.0	CeO_2	8.7
			529.8	MnO_2	61.1
			531.1	OH	6.3
			531.7	C=O (COOR)	7.0
			532.5	H_2O	4.1
			533.5	C–O (C–OH; COOR)	12.7

$C_2H_6^+/CHOH^+ = m/z$ 30; $CH_3O^+ = m/z$ 31, and finally $K^+/C_3H_3^+ = m/z$ 39 (17, 45–47). Potassium cations, if present may originate from impurities present in sodium hydroxide used during the catalyst preparation. Because of the low mass resolution of the S-SIMS instrument used, it was impossible to discriminate unambiguously between different species having the same nominal mass but different exact masses. The relative peak intensity ratios for the detected ions are summarized in Table 6 for short and long reaction times. According to Albers *et al*. (40, 48), the positively charged fragment ions such as CH_x^+ ($x = 1-3$) indicate the presence of long-chain aliphatic surface compounds. Consequently, as seen in Table 6, the elevated ratios for $\sum CH_x^+$ to C_2^+ observed for all CWO temperatures (mean value = 100.4) indicate the presence of long aliphatic chains in the carbonaceous deposit. The C_2 m/z 25–28) hydrocarbon fragments also exhibited high relative intensities, the highest values being attributed to $C_2H_3^+$. In general, the relative intensity for this fragment ion was higher at the lowest CWO temperature. Moreover, the relative intensity increased with CWO reaction time for most temperatures. The same trend was observed for $C_3H_3^+$. The oxygen-containing ions CHO^+ (mean value of ca. 240) gave more intense signals than $CHOH^+$ and CH_2OH^+ (mean values of ca. 20 and 30, respectively).

Negative Ion Spectra

The negative ion spectra (m/z 0–40) of the used MnO_2/CeO_2 catalyst in CWO reactions at different temperatures and after achieving complete TOC conversion are given in Fig. 11. The strong peaks observed at m/z 12–15, 16, and 17 were attributed to CH_x^- ($x = 0-3$), O^-, and OH^- ions, respectively. The signals CH_x^- ($x = 1-2$) are a good indicator of the chemically bonded hydrogen in partially hydrogenated or hydrogen-rich surface regions (40). There were also peaks at m/z 24 and 25 that were assigned to C_2^- and C_2H^- ions. The relative intensities of some characteristic negative ions are given in Table 7 for short and long reaction times. Assuming that the C_2H^-/C_2^- ratios are a rough estimate for the hydrogen content of these deposits, graphitization leads to a decrease in the total hydrogen content and to a simultaneous decrease in the relative intensity of the C_2H^- signal. In fact, low C_2H^-/C_2^- ratios were observed for hydrogen-deficient graphitized surfaces (40, 49). In the current study, the mean value obtained for this ratio was 2.66, which is characteristic of low-polycondensation aromatics ($\leq$4 condensed aromatic rings). Indeed, for a model benzofluoranthene molecule (four condensed aromatic rings

TABLE 6

Ratio to C_2^+ of Positive SIMS Peaks

CWO Temp (°C)	Time (min)	$\sum(CH_x^+)$	C_2H^+	$C_2H_2^+$	$C_2H_3^+$	$C_2H_4^+$	$C_2H_5^+$ (CHO^+)	$C_2H_6^+$ ($CHOH^+$)	CH_2OH^+	$C_3H_3^+$
80	5	90.6	1.5	30.6	319.4	67.3	259.6	21.4	26	60
90	5	54.7	0.4	15.1	168.3	31.1	139.6	8.6	9.8	52.5
110	5	74.3	1.1	23.9	241.8	49.6	177.9	18.6	19	67.2
130	1.5	48.4	0.7	12.0	80.6	16.1	58.4	7.0	8.1	58.3
80	75	304.0	9.0	142.0	1105.0	166.0	827.0	64.0	107	310
90	90	48.6	2.2	30.2	183.6	37.8	120.2	17.2	9.9	78.2
110	90	18.5	0.6	9.5	72.0	17.4	50.9	7.7	6.8	49.4
130	30	164.3	2.0	38.0	414.3	55.8	284.0	17.8	39	482

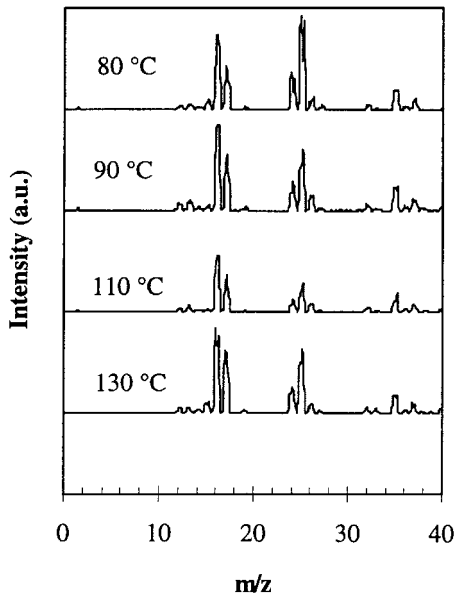

FIG. 11. S-SIMS spectra for catalyst samples withdrawn at different CWO temperatures: Negative secondary ions.

and one 5-carbon ring), this ratio was found to be equal to 2.20 (50). Generally, regardless of the CWO temperature, this ratio decreased at long reaction times (i.e., evolution to a higher level of aromatic ring condensation). This is in agreement with the XPS findings that showed an increase in the contribution of graphitic/aromatic carbon with CWO reaction time at all oxidation temperatures investigated.

CONCLUSION

The deactivating carbonaceous material adsorbed on MnO_2/CeO_2 catalyst surface during the course of CWO reaction was characterized using three different techniques, TPO–MS, XPS, and S-SIMS. The first technique revealed that these carbonaceous deposits exhibit complex structure with components burning at different temperatures between 200 and 300°C. The first species burning at the lowest temperature were shown to be poorly hydrogenated or nonhydrogenated. TPO–MS analysis performed on catalyst samples withdrawn at different stages of CWO reaction showed that the composition and the amount of the carbonaceous material evolved during the course of the reaction. The XPS analysis confirmed the occurrence of a carbonaceous overlayer on the catalyst surface during the CWO reaction, as the amount of surface carbon increased with CWO reaction time. Peak reconstruction and curve fitting performed on the multicomponent C1*s* peak revealed the presence of aromatic/graphitic and oxygenated aliphatic species as well as oxygen-containing compounds from alcohol/ether origin. The composition of the deposits was reaction time and temperature dependent. The main observations were: (i) the highest contribution was from the oxygenated aliphatics, (ii) the contribution of the aromatic/graphitic signal increased with CWO reaction time for all CWO temperatures, and (iii) this later contribution decreased linearly with temperature. The O1*s* peak analysis revealed a strong contribution of oxygen originating mainly from Mn oxide and an increase in the organic oxygen as reaction time increased. The S-SIMS data revealed the existence of aliphatic chains on the used catalyst surface and suggested low polycondensation of the deposits, evaluated to be approximately 4 condensed aromatic rings.

TABLE 7

Ratio to C_2^- Peak of Negative SIMS Peaks

CWO Temp. (°C)	Time (min)	C^-	CH^-	CH_2^-	CH_3^-	C_2H^-	$C_2H_2^-$
80	5	0.22	0.33	0.28	1.22	3.56	1.61
90	5	0.18	0.46	0.36	0.50	2.43	0.79
110	5	0.24	0.41	0.21	0.38	2.10	0.69
130	1.5	0.24	0.33	0.16	0.38	3.05	0.95
80	75	0.14	0.18	0.10	0.30	2.94	0.34
90	90	0.24	0.37	0.09	0.15	2.32	0.59
110	90	0.29	0.44	0.15	0.17	2.40	0.68
130	30	0.15	0.24	0.17	0.43	2.44	0.27

ACKNOWLEDGMENTS

Financial support from the Natural Sciences and Engineering Research Council of Canada (NSERC) and the Fonds pour la Formation de Chercheurs et d'Aide à la Recherche (Québec) is gratefully acknowledged. The authors thank Professor B. Grandjean for the use of the Leybold mass spectrometer.

REFERENCES

1. Levec, J., *Chem. Biochem. Eng. Q.* **11**, 47 (1997).
2. Sadana, A., and Katzer, J. R., *J. Catal.* **35**, 140 (1974).
3. Ohta, H., Goto, S., and Teshima, H., *Ind. Eng. Chem. Fundam.* **19**, 180 (1980).
4. Pintar, A., and Levec, J., *J. Catal.* **135**, 345 (1992).
5. Matatov-Meytal, Y. I., and Sheintuch, M., *Ind. Eng. Chem. Res.* **37**, 309 (1998).
6. Hamoudi, S., Larachi, F., and Sayari, A., *J. Catal.* **177**, 247 (1998).
7. Hamoudi, S., Larachi, F., Cerrella, G., and Cassanello, M., *Ind. Eng. Chem. Res.* **37**, 3561 (1998).
8. Li, C., Minh, C. L., and Brown, T. C., *J. Catal.* **178**, 275 (1998).
9. Augustine, S. M., Alameddin, G. N., and Sachtler, W. M. H., *J. Catal.* **115**, 217 (1989).
10. Menon, P. G., *J. Mol.Catal* **59**, 207 (1990).
11. Barr, T. L., and Yin, M., *J. Vac. Sci. Technol. A* **10**, 2788 (1992).
12. Affrossman, S., Comrie, R. F., and Mac Donald, S., *J. Chem. Soc. Faraday Trans.* **94**, 289 (1998).
13. Affrossman, S., and Mac Donald, S., *Langmuir* **12**, 2090 (1996).
14. Leggett, G. J., Davies, M. C., Jackson, D. E., and Tendler, S. J. B., *J. Chem. Soc. Faraday Trans. 1* **89**, 179 (1993).
15. Niemantsverdriet, J. W., and van Langeveld, A. D., *Fuel* **65**, 1396 (1986).

16. Menon, P. G., *Chem. Rev.* **94**, 1021 (1994).
17. Weng, L. T., Bertrand, P., Stone-Masui, J. H., and Stone, W. E. E., *Langmuir* **13**, 2943 (1997).
18. Imamura, S., Dol, A., and Ishida, S., *Ind. Eng. Chem. Prod. Res. Dev.* **24**, 75 (1985).
19. Hughes, A. H., and Sexton, B. A., *J. Electron Spectr.* **46**, 31 (1988).
20. Cumpson, P. J., and Seah, M. P., *Surf. Interface Anal.* **21**, 274 (1994).
21. Gengenbach, T. R., Chatelier, R. C., and Griesser, H. J., *Surf. Interface Anal.* **24**, 271 (1996).
22. Desimoni, E., Casella, G. I., Morone, A., and Salvi, A. M., *Surf. Interface Anal.* **15**, 627 (1990).
23. Paàl, Z., Schlögl, R., and Ertl, G., *Catal. Lett.* **12**, 331 (1992).
24. Darmstadt, H., Roy, C., and Kaliaguine, S., *Carbon* **32**, 1399 (1994).
25. Wagner, C. D., Zatko, D. A., and Raymond, R. H., *Anal. Chem.* **52**, 1445 (1980).
26. Bensalem, A., Bozon-Verduraz, F., Delamar, M., and Bugli, G., *Appl. Catal. A: Gen.* **121**, 81 (1995).
27. Paàl, Z., Schlögl, R., and Ertl, G., *J. Chem. Soc. Faraday Trans. I* **88**, 1179 (1992).
28. Dias, C. R., Portela, M. F., and Bond, G. C., *Stud. Surf. Sci. Catal.* **88**, 475 (1994).
29. Wagner, C. D., Riggs, W. M., Davis, L. E., Moulder, J. F., and Muilenberg, G. E., "Handbook of X-Ray Photoelectron Spectroscopy." Perkin–Elmer Corporation, Physical Electronics Division, Eden Prairie, MS, 1979.
30. Barr, T. L., Fries, C. G., Cariati, F., Bart, J. C. J., and Giordano, N., *J. Chem. Soc. Dalton Trans.* 1825 (1983).
31. Nefedov, V. I., Gati, D., Dzhurinskii, B. F., Sergushin, N. P., and Salyn, Y. V., *Zh. Neorg. Khim.* **20**, 2307 (1975).
32. Sarma, D. D., and Rao, C. N. R., *J. Electron Spectrosc. Relat. Phenom.* **20**, 25 (1980).
33. Imamura, S., Nakamura, M., Kawabata, N., Yoshida, J., and Ishida, S., Ind. Eng. *Chem. Prod. Res. Dev.* **25**, 34 (1986).
34. Oku, M., Hirokawa, K., and Ikeda, S., *J. Electron Spectrosc.* **7**, 465 (1975).
35. Carver, J. C., Schweitzer, G. K., and Carlson, T. A., *J. Chem. Phys.* **57**, 980 (1972).
36. Aoki, A., *Jpn. J. Appl. Phys.* **15**, 305 (1976).
37. Burroughs, P., Hamnett, A., Orchard, A. F., and Thornton, G., *J. Chem. Soc. Dalton Trans.* 1686 (1976).
38. Creaser, D. A., Harrison, P. G., Morris, M. A., and Wolfindale, B. A., *Catal. Lett.* **23**, 13 (1994).
39. Mason, R. L., Gunst, R. F., and Hess, J. L., "Statistical Design and Analysis of Experiments with Applications to Engineering and Science." p. 530. Wiley, New York, 1989.
40. Albers, P., Deller, K., Despeyroux, B. M., Schäfer, A., and Seibold, K., *J. Catal.* **133**, 467 (1992).
41. Kelemen, S. R., Rose, K. D., and Kwiatek, P. J., *Appl. Surf. Sci.* **64**, 167 (1993).
42. Matolin, V., Gillet, E., and Channakhone, S., *J. Catal.* **97**, 448 (1986).
43. Sellmer, C., Prins, R., and Kruse, N., *Catal. Lett.* **47**, 83 (1997).
44. Rehbolz, M., and Kruse, N., *J. Chem. Phys.* **95**, 7745 (1991).
45. Hammerton, I., Hay, J. N., Howlin, B. J., Jones, J. R., Lu, S., and Webb, G. A., *Chem. Mater.* **9**, 1973 (1997).
46. Shard, A. G., Davies, M. C., Tendler, S. J. B., Bennedetti, L., Purbrick., M. D., Paul, A. J., and Beamson, G., *Langmuir* **13**, 2909 (1997).
47. Petrat, F. M., Wolany, D., Schede, B. C., Wiedman, L., and Benninghoven, A., *Surf. Interface Anal.* **21**, 474 (1994).
48. Albers, P., Deller, K., Despeyroux, B. M., Prescher, G., Schäfer, A., and Seibold, K., *J. Catal.* **150**, 368 (1994).
49. Ashida, K., Kanamori, K., and Watanabe, W., *J. Vac. Sci. Technol. A* **6**, 2232 (1988).
50. Darmstadt, H., Chaala, A., Roy, C., and Kaliaguine, S., *Fuel* **75**, 125 (1996).

.